Thermal Energy Transfer Across Solid of (110) Crystal Plane in Contact with Ultra-thin Liquid Film

Abdul Rafeq bin Saleman[1*], Mohamad Shukri bin Zakaria[1], Ridhwan bin Jumaidin[2], Azwan Sapit[3], Mohd Azahari bin Razali[3]

[1] Fakulti Kejuruteraan Mekanikal, Universiti Teknikal Malaysia Melaka, Malaysia

[2] Fakulti Teknologi Kejuruteraan Mekanikal dan Pembuatan, Universiti Teknikal Malaysia Melaka, Malaysia

[3] Fakulti Kejuruteraan Mekanikal dan Pembuatan, Universiti Tun Hussien Onn, Malaysia

ABSTRACT

The non-equilibrium molecular dynamics (NEMD) simulation of ultra-thin liquid film of solid in contact with liquid film has been examined. A high temperature and low temperature has been applied respectively on the left and right sides of the solids, creates a constant heat flux throughout the simulation system. The effect of different liquid film thicknesses on the interfacial thermal resistance (ITR) at the contact interfaces of solid and liquid or interfaces of solid-liquid (S-L) has also been investigated. Different structural quantities have been observed for varied liquid film thicknesses. The oscillation of the density profile for liquid near solid surfaces decreases with the decrease in liquid film thickness. The ITR is calculated from the temperature discontinuity and heat flux near the contact interfaces of S-L. It has been discovered that although the temperature discontinuity near the interfaces of S-L is approximately the same, the ITR is significantly influenced by the thickness of the liquid film. According to the results, it has been understood that the smaller the thickness of the liquid film, the higher the thermal energy transfer across the interfaces of S-L.

KEYWORDS: *solid-liquid interfaces, molecular dynamic simulation, lubrication and coating system*

1.0   INTRODCUTION

Solid-liquid (S-L) interfaces refer to contact interfaces between solid surfaces and liquid. This has been established in a number of engineering applications such as in lubrications and coatings for automotive applications (Abdullah, Abdollah, Amiruddin, Nuri, et al., 2014; Abdullah, Abdollah, Amiruddin, Tamaldin, et al., 2014; Nazri et al., 2013), thermal interface materials (Prasher, 2006), and electronic cooling (Choi et al., 2002; Wang et al., 2012). In most of the mentioned examples, the systems will fail without an adequate thermal management system. As such, it is crucial to understand the nature of heat and momentum transport to optimize and control the performance of the system. In recent years, due to the development of nanotechnologies (Apóstolo et al., 2019; Dandan et al., 2018; Hamdan et al., 2018), researcher are now keen to examine the problem at a molecular level. However, the system would be anomalous and cannot be determined or predicted by the normal macroscopic concept. For such a

problem, molecular dynamics simulation is a promising tool that can be used to mimic the phenomenon of molecular for an extensive analysis.

In the past several years, numerous investigations have been accomplished on heat and momentum transport (Liu et al., 2020; A. R. Saleman et al., 2018; A. R. bin Saleman et al., 2017). Some had looked into the molecular interaction between solid and liquid by using simple liquid (T. Ohara & D.Suzuki, 2000; Torii et al., 2010) or liquid with straight chain molecules (A. R. bin Saleman et al., 2017). Understanding this phenomenon may help in designing proper thermal management systems at contact interfaces of automotive applications or even optimize the design of electronic systems.

Several previous studies had examined thermal energy transfer (Kikugawa et al., 2009; Matsubara et al., 2015; Ohara & Torii, 2005), however, the influences of liquid film thickness in regard to thermal energy transfer still requires further assessment. Therefore, this study analyses the impact of liquid film thickness on thermal energy transfer at the interfaces of S-L. The effect of different liquid film thicknesses is assessed based on the structural quantities and ITR at the interfaces of S-L. To verify the result, three different liquid film thicknesses (10 Å, 30 Å, and 60 Å) have been tested in this study.

2.0   METHODOLOGY PREPARATION

2.1   Model Development

(a) Simulation model
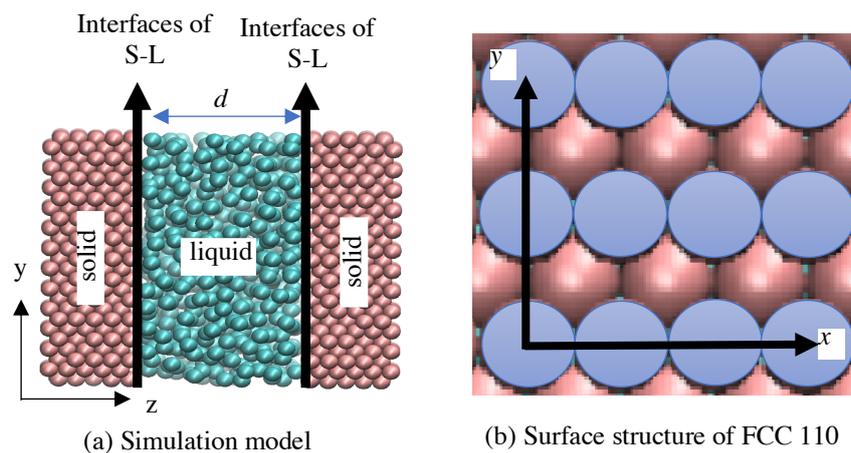
(b) Surface structure of FCC 110

Figure 1.(a) Simulation model and (b) surface structure FCC110.

The model of this simulation contains an extremely thin liquid film enclosed between two identical solid walls, as shown in Figure 1 (a). The solid consists of gold (Au) with face-centered cubic (FCC) crystal plane of 110 and in contact with liquid methane, as shown in Figure 1 (b). An identical surfaces of crystal plane was employed on the left and right sides of the solid walls in contact with the liquid film. This study analyzes the thicknesses of 10 Å, 30 Å, and 60 Å of liquid film, *d*. The sizes of the simulation system in the *x*- and *y*-directions are 46 Å and 48 Å, respectively, regardless of the liquid film thickness. For the *z*-direction, the sizes are 68 Å, 88 Å, and 118 Å for 10 Å, 30 Å, and

60 Å liquid film thicknesses, respectively. A periodic boundary condition is put on to the simulation system in the *x*- and *y*-directions. The simulation was set to be fixed in the *z*-direction as to make sure that the simulation model did not drifted during simulation. Such a model represents the solid wall as part of an extremely large solid.

2.2 Potential Functions

The solid walls were modelled by Morse potentials. The same potentials were employed in previous studies (Liu et al., 2020; Rafeq et al., 2018; A. R. B. Saleman et al., 2019). The potential function is given in eqn (1)

$$\Phi(r_{ij}) = D[e^{-2\alpha(r_{ij}-r_o)} - 2e^{-\alpha(r_{ij}-r_o)}] \tag{1}$$

Based on Equation (1), $D = 7.6148 \times 10^{-20}$, $r_o = 3.0242$ Å, and $\alpha = 1.580$ Å^{-1} (Rafeq et al., 2018).

The liquid methane was modelled by the united atom. In this model, carbon atom and hydrogen atoms were combined as a single interaction site at the centre of carbon atom which being called as pseudo atom. The interaction force between each pseudo atom, which is the potential function, was modelled by the Transferable Potential for Phase Equilibria (TraPPE) force field (Martin & Siepmann, 1998). The parameters for the interaction force were developed using Lennard Jones 12-6 (LJ) potentials. The potential function is given as in eqn (2)

$$U^{LJ}(r_{ij}) = 4\varepsilon_{ij}\left[\left(\frac{\sigma_{ij}}{r_{ij}}\right)^{12} - \left(\frac{\sigma_{ij}}{r_{ij}}\right)^{6}\right] \tag{2}$$

The distance of pseudo atoms *i* and *j* is r_{ij}. ε_{ij} and σ_{ij} is 2.0433×10^{-21} and 3.73 Å, respectively, which are the energy parameter of the interaction force between *i* and *j* (Martin & Siepmann, 1998; Müller & Mejía, 2011).

The interaction between Au solid and methane liquid was displayed by Lorentz-Berthelot combining rules, the energy parameters of the ε_{sl} and σ_{sl} were calculated as:in eqn (3)

$$\varepsilon_{sl} = \sqrt{\varepsilon_{ss}\varepsilon_{ll}} \quad \text{and} \quad \sigma_{sl} = \frac{\sigma_{ss} + \sigma_{ll}}{2} \tag{3}$$

The *s* and *l* refer to Au solid and methane liquid, respectively. The ε_{sl} and σ_{sl} for the solid atom is 2.7109×10^{-21} and 3.70 Å, respectively (Martin & Siepmann, 1998; Müller & Mejía, 2011). In this simulation, the potential function is truncated at the cuff-off radius of 12.0 Å (A. R. bin Saleman et al., 2017).

2.3 Simulation methods

The time integration method for this simulation system were the reversible Reference Propagator Algorithm (r-RESPA) with manifold timesteps. One femto second have been applied to the molecular motion between two molecules. And 0.2 femto second of time integration have been applied for molecular motion within each atom/pseudo atom in a molecule.

Initially a targeted temperature at 0.7 of the liquid's critical temperature was set in the simulation system. Then the system's temperature was raised up slowly until a uniform

and constant temperature was acquired throughout the simulation system (0.7 of the liquid's critical temperature). The uniform temperature was equilibrated for 1 to 4 million timesteps. Next, a constant heat flux was applied across the simulation system. The heat flux setup was established by using the velocity scaling method where a high temperature was set on the solid wall of the left side and a low temperature was set on the solid wall of the right side of the simulation system. The temperature different developed a constant heat flux across the simulation system. The constant heat flux setup was applied to the simulation system for another 1 to 4 million timesteps for equilibrium. Finally, the data collection step for 10 to 20 million timesteps was applied to the simulation system where the density, temperature, and heat flux data have been successfully recorded.

3.0   RESULTS AND DISCUSSIONS

3.1   Density Distributions

As known in the past studies density distributions play a significant role in giving the insight of the molecular behaviour (Chilukoti et al., 2016; A. R. bin Saleman et al., 2017). In this study, to calculate the density distribution, the simulation system was first evenly cut into 6000 number of rectangular slabs in the z-direction. The number of molecules/atom present in each evenly cut slab was then determined. The number of molecules/atoms in each evenly cut slab was then converted into the unit of kg/m^3 by using Avogadro number and molar mass of the molecules/atoms. Figure 2 presents the density distribution for the simulation model with liquid film thicknesses of 10 Å (red), 30 Å (green), and 60 Å (blue).

As known in previous research (A. R. b. Saleman et al., 2017; A. R. bin Saleman et al., 2017), the density distribution of liquid oscillates near the solid wall, and the oscillation here refers to the adsorption layer of the liquid. A straight or flat line was observed at the center of the simulation system, also known as the bulk-like region (A. R. bin Saleman et al., 2017). The same profile of density distributions is observed in Figure 3 (c). Since the same simulation model and number of molecules have been utilized in previous study in ref (A. R. b. Saleman et al., 2017; A. R. bin Saleman et al., 2017), the simulation model for L_z of 60 Å is considered validated.
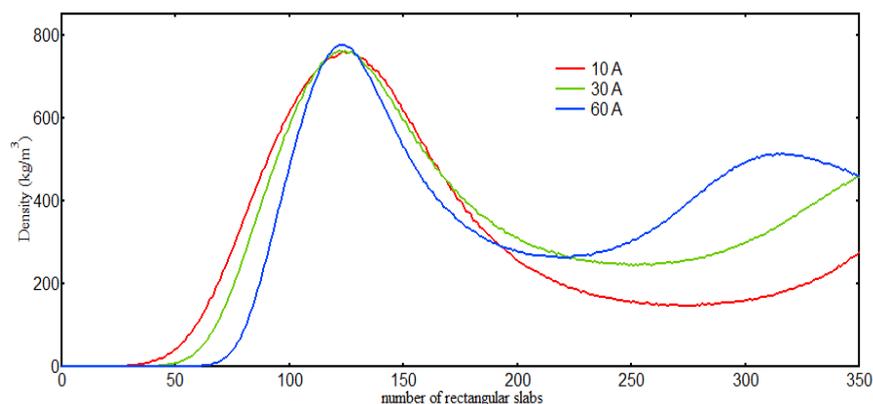

Figure 2. First adsorption layer for simulation model with liquid film thicknesses of 10 Å (red line), 30 Å (green line), and 60 Å (blue line).
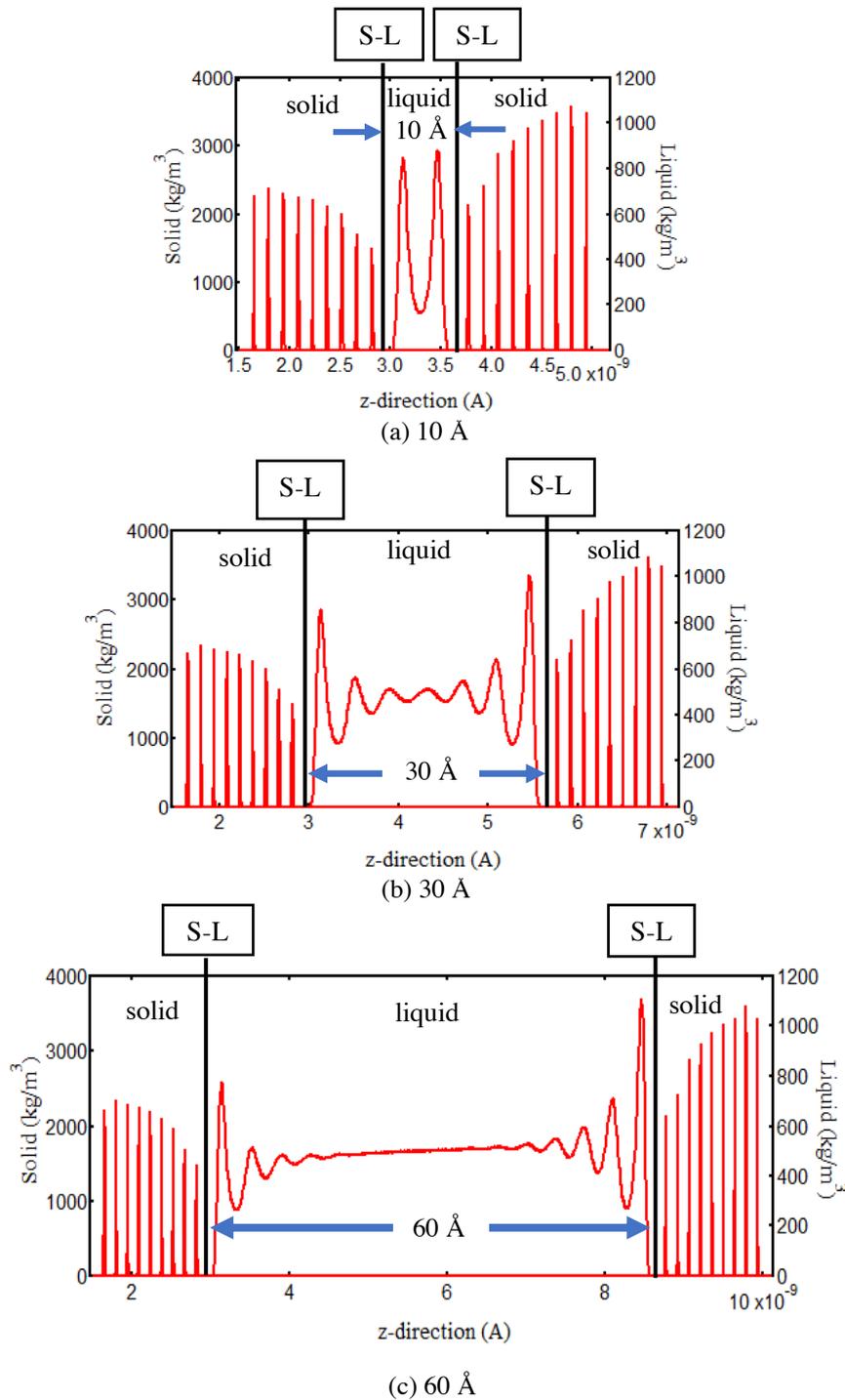
(a) 10 Å

(b) 30 Å

(c) 60 Å

Figure 3. Density distributions for simulation model with liquid thicknesses of (a) 10 Å, (b) 30 Å, and (c) 60 Å.

In order to compare the results between the simulation systems, the adsorption layer of the liquid which was the closest to the left side of the simulation system was controlled in a way that the peak height was approximately equal at the same temperature, as shown in Figure 2 (for the peak height) and Figure 5 (for the temperature of the liquid nearest to the interfaces of S-L on the left side of the simulation system). The same method was utilized to identify the number of molecules for each simulation system

with the comparison also shows that the simulation system for L_z of 10 Å and 30 Å were validated. This is the only method to effectively compare between the simulation systems.

Figure 3 displays the density distributions of the current simulation system for the liquid film thicknesses of 10 Å, 30 Å, and 60 Å. As observed in Figure 3, different density distributions have been observed for different liquid film thicknesses. For the case of 60 Å, a bulk-like region exists at the center of the simulation system. This existence indicates that there was no interaction force by the two identical solid walls at the center of the simulation system (or at the center of the liquid film). However, for the cases of 30 Å and 10 Å, no bulk-like region was present at the center of both simulation systems. Based on these results, it is understood that the liquid film thickness significantly influences the structure of the density distributions. In addition, a decrease in liquid film thickness further decreases the number of adsorption layers. Based on Figure 3, the peak height of the first adsorption layer on the right side is not at the same height. This is due to the influences of temperature which have been imposed on the left and right side of the simulation system (temperature left and right tak sama?) as well as the constant amount of heat flux applied across all simulation cases.

3.2   Temperature Distributions

A well-defined slab was established as shown in Figure 4 to calculate the temperature of the simulation system. The slab definition is based on the position of the valley of the density distributions. The same definition of slabs was utilized in a previous study (A. R. b. Saleman et al., 2017). The green vertical line represents the border of each slab. Since the simulation system is symmetrical, only the slab definition on the left side is shown in Figure 4**.** The temperature for each slab was calculated based on the summation of the microscopic velocity of each molecule/atom present in each slab.
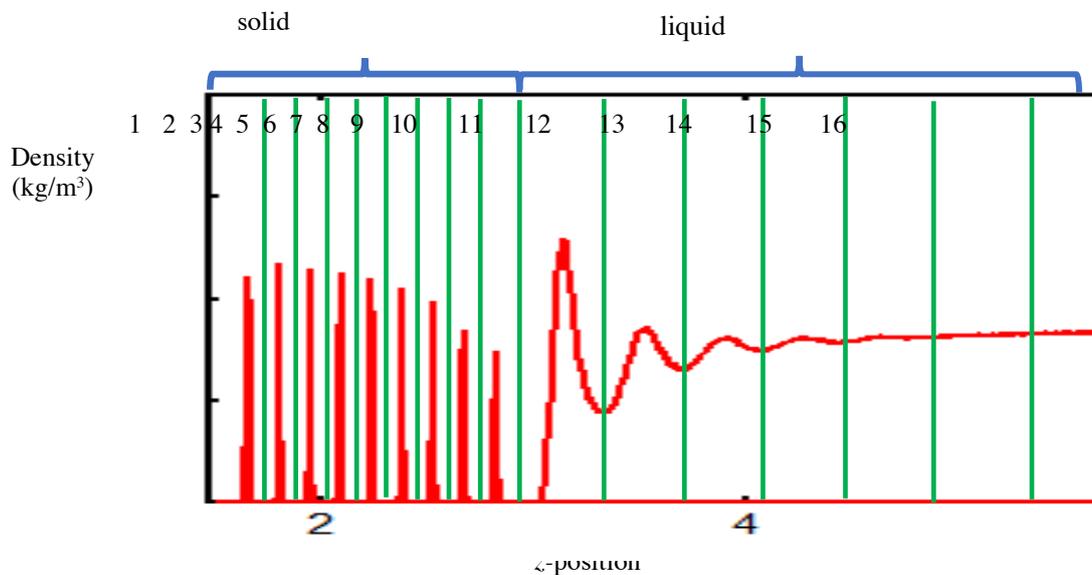

Figure 4. Slab definition for temperature distributions
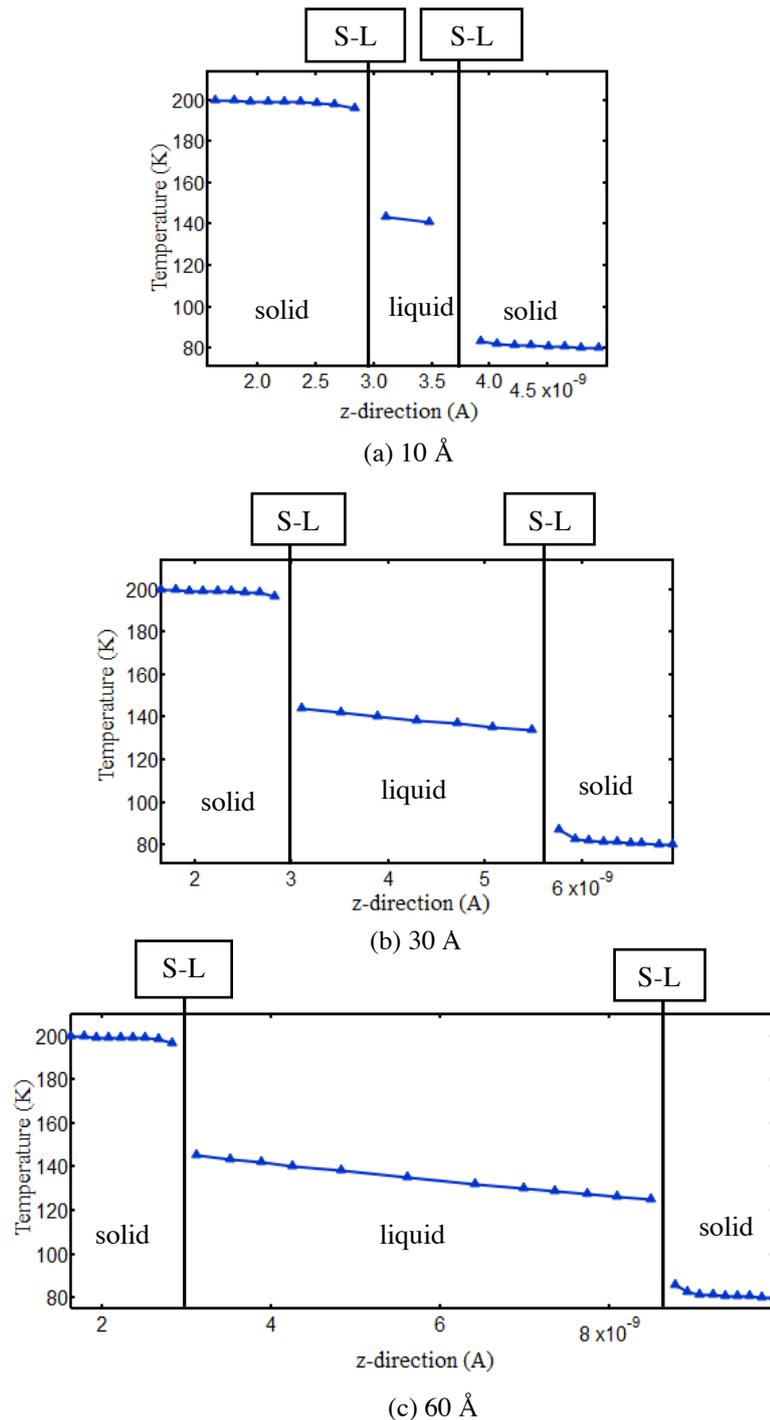
(a) 10 Å

(b) 30 A

(c) 60 Å

Figure 5. Temperature distribution for liquid film thicknesses for(a) 10 Å, (b) 30 Å, and (c) 60 Å.

Figure 5 presents the temperature distributions for liquid film thicknesses of 10 Å, 30 Å, and 60 Å. In this study, only the left side of the simulation system was compared among all cases since only the left sides have been controlled at the same reduced temperature. As observed, a temperature discontinuity does exist at the interfaces of S-L regardless of the liquid film thickness (10 Å, 30 Å, and 60 Å). The same behaviour was observed in previous studies (Liu et al., 2020; Rafeq et al., 2018; A. R. Saleman et al., 2018). This is due to the phonon mismatch at the contact interface of the solid and liquid (Barrat & Chiaruttini, 2002; Torii et al., 2008). The temperature discontinuity is referred to as

temperature jump (TJ) after this. The TJ is evaluated as the temperature of the outermost layer of the liquid and inner most layer of the solid extrapolated to the position of the interfaces of S-L. The interfaces of S-L is assumed to be exactly at the center between the Au solid and methane liquid. The temperature difference between the Au solid and methane liquid is then determined. The same method was employed in previous studies (A. R. Saleman et al., 2018; A. R. bin Saleman et al., 2017).

3.3   Interfacial Thermal Resistance (ITR)

Irvng-Kirkwood was the one derived the equation to determine the heat flux (HF) throughout the simulation in this study. The details of the equation can be found in the literature (A. R. B. Saleman et al., 2019; A. R. bin Saleman et al., 2017; Torii et al., 2008). In order to validate the simulation results, the thermal conductivity of the liquid in the simulation were compared to the experimental value. The thermal conductivity for the experimental value tabulated in Table 1 were obtained from the correlation formula proposed by Assael et. al. (Assael et al., 1992). As for the current simulation, the value of thermal conductivity is determined from the temperature difference of the liquid and the constant heat flux applied across the simulation system. It is found that the deviation in percentage between the current simulation and experiment value of thermal conductivity for d of 10 Å is 13%, for d of 30 Å is 9% and for d of 60 Å is 11%. Considering the deviation, the molecular dynamics simulation successfully reproduces the thermal conductivity of the liquid alkanes. The differences in the value of thermal conductivity between each of the simulation system is due to size of the simulation system and the value of the density. As observed in Figure 2, there are slight differences in the peak height between the d of 10 Å, 30 Å, and 60 Å. As such, the number of molecules is not exactly accurate, however such inaccuracy is still within the acceptable limit.

Table 1 Thermal conductivity from present simulation system

d (Å)	W /m . K		Deviation in percentage
	Experimental value (Assael et al., 1992)	Current simulation	
10		1.28×10^{-1}	13%
30	1.47×10^{-1}	1.61×10^{-1}	9%
60		1.63×10^{-1}	11%

Table 2 displays the values of the TJ, heat flux (HF), and Interfacial Thermal Resistance (ITR). Based on Table 2, the TJ is approximately the same regardless of the liquid film thickness: 50.91 K, 52.17 K, and 50.73 K for 10 Å, 30 Å, and 60 Å, respectively. The TJ is found to have approximately the same value which is due to the surface structure of (110) crystal plane as shown in Figure 1 (b). On the surface of (110) crystal plane there exists surface corrugation, which absorbed methane molecules (liquid) inside it. The adsorbed methane molecules (liquid) did not fluctuate much and as a result, approximately similar TJ is observed regardless the liquid film thickness. Although the TJ is approximately similar, the HF for each case of liquid film thickness across the simulation system is completely different. The HF was in the order of 10 Å, 30 Å, and 60 Å, starting from the highest to the lowest value. Based on the TJ and HF data, the interfacial thermal resistance (ITR) was calculated, which is a ratio of TJ to HF. Although the peak height of the outermost layer of liquid and the

reduced temperature for each case of the simulation system are approximately equal, the ITR at the S-L interfaces was different. Based on the figure, the ITR decreased with the decrease in liquid film thickness. The same pattern have been observed in previous study (Liu et al., 2020). The ITR is correlated to the number of adsorption layers appearing on the density profile of the liquid. The lesser the number of adsorption layers, the lower the value of ITR at the interfaces of S-L.

Table 2 TJ, heat flux (HF), and interfacial thermal resistance (ITR) for 10 Å, 30 Å, and 60 Å

d (Å)	TJ (K)	HF x 10^6 (MW)	ITR x 10^{-8} (K/W)
10	50.91	733.7	6.9387
30	52.17	688.4	7.5795
60	50.73	605.7	8.3751

4.0   CONCLUSION

This study investigated the influence of liquid film thickness of two identical solid walls in contact with liquid. It was found that the density profile behaves differently whenever the liquid film thickness decreases. The existence of a bulk-like region, as found in previous studies, did not appear in these results for the extremely thin liquid films with thicknesses of 10 Å and 30 Å. Based on the results, can be assumed that the liquid film thickness and density profile influence the characteristics of ITR at the S-L interfaces where the thinner the liquid film thickness, the lower the ITR at the interfaces of S-L.

5.0   REFERENCES

Abdullah, M. I. H. C., Abdollah, M. F. B., Amiruddin, H., Nuri, N. R. M., Tamaldin, N., Hassan, M., & Rafeq, S. A. (2014). Effect of hBN/Al2O3 nanoparticles on engine oil properties. *Energy Education Science and Technology Part A: Energy Science and Research*, *32*(5), 3261–3268.

Abdullah, M. I. H. C., Abdollah, M. F. B., Amiruddin, H., Tamaldin, N., Nuri, N. R. M., Hassan, M., & Rafeq, S. A. (2014). Improving engine oil properties by dispersion of hBN/Al2O3 nanoparticles. In *Applied Mechanics and Materials* (Vol. 607). https://doi.org/10.4028/www.scientific.net/AMM.607.70

Apóstolo, R. F. G., Tsagkaropoulou, G., & Camp, P. J. (2019). Molecular adsorption, self-assembly, and friction in lubricants. *Journal of Molecular Liquids*, *277*, 606–612. https://doi.org/10.1016/j.molliq.2018.12.099

Assael, M. J., Dymond, J. H., Papadaki, M., & Patterson, P. M. (1992). Correlation and prediction of dense fluid transport coefficients. I. n-alkanes. *International Journal of Thermophysics*, *13*(2), 269–281. https://doi.org/10.1007/BF00504436

Barrat, J. L., & Chiaruttini, F. (2002). Kapitza resistance at the liquid-solid interface. *Molecular Physics*, *101*, 1605–1610. https://doi.org/10.1080/0026897031000068578

Chilukoti, H. K., Kikugawa, G., & Ohara, T. (2016). Structure and Mass Transport Characteristics at the Intrinsic Liquid-Vapor Interfaces of Alkanes. *Journal of Physical Chemistry B*, *120*(29), 7207–7216. https://doi.org/10.1021/acs.jpcb.6b05332

Choi, J., Kawaguchi, M., & Kato, T. (2002). Self-assembled monolayer formation on magnetic hard disk surface and friction measurements. *Journal of Applied Physics*, *91*(2002), 7574–7576. https://doi.org/10.1063/1.1452690

Dandan, M. A., Aiman Wan Yahaya, W. M., Samion, S., & Musa, M. N. (2018). A comprehensive review on palm oil and the challenges using vegetable oil as lubricant base-stock. *Journal of Advanced Research in Fluid Mechanics and Thermal Sciences*, *52*(2), 182–197.

Hamdan, S. H., Chong, W. W. F., Ng, J. H., Chong, C. T., & Zhang, H. (2018). Nano-tribological characterisation of palm oil-based trimethylolpropane ester for application as boundary lubricant. *Tribology International*, *127*(May), 1–9. https://doi.org/10.1016/j.triboint.2018.05.036

Kikugawa, G., Ohara, T., Kawaguchi, T., Torigoe, E., Hagiwara, Y., & Matsumoto, Y. (2009). A molecular dynamics study on heat transfer characteristics at the interfaces of alkanethiolate self-assembled monolayer and organic solvent. *The Journal of Chemical Physics*, *130*(7), 074706. https://doi.org/10.1063/1.3077315

Liu, X., Surblys, D., Kawagoe, Y., Bin Saleman, A. R., Matsubara, H., Kikugawa, G., & Ohara, T. (2020). A molecular dynamics study of thermal boundary resistance over solid interfaces with an extremely thin liquid film. *International Journal of Heat and Mass Transfer*, *147*, 118949. https://doi.org/10.1016/j.ijheatmasstransfer.2019.118949

Martin, M. G., & Siepmann, J. I. (1998). Transferable potentials for phase equilibria. 1. united-atom description of n -alkanes. *The Journal of Physical Chemistry B*, *102*(97), 2569–2577. https://doi.org/10.1021/jp972543+

Matsubara, H., Kikugawa, G., Bessho, T., Yamashita, S., & Ohara, T. (2015). Effects of molecular structure on microscopic heat transport in chain polymer liquids. *Journal of Chemical Physics*. https://doi.org/10.1063/1.4919313

Müller, E. a., & Mejía, A. (2011). Comparison of united-atom potentials for the simulation of vapor-liquid equilibria and interfacial properties of long-chain n-alkanes up to n-C 100. *Journal of Physical Chemistry B*, *115*, 12822–12834. https://doi.org/10.1021/jp203236q

Nazri, Z. H., Rody, M. Z. M., Abdollah, M. F. B., Rafeq, S. A., Amiruddin, H., Tamaldin, N., & Masripan, N. A. B. (2013). Elastohydrodynamics lubrication for bio-based lubricants in elliptical conjunction. *Procedia Engineering*, *68*. https://doi.org/10.1016/j.proeng.2013.12.157

Ohara, T., & Torii, D. (2005). Molecular thermal phenomena in an ultrathin lubrication liquid film of linear molecules between solid surfaces. *Microscale Thermophysical Engineering*, *9*(3), 265–279. https://doi.org/10.1080/10893950500196386

Prasher, R. (2006). Thermal interface materials: historical perspective, status, and future directions. *Proceedings of the IEEE*, *94*(8), 1571–1586. https://doi.org/10.1109/JPROC.2006.879796

Rafeq, A., Saleman, B., Munir, F. A., Fadzli, M., Abdollah, B., Kikugawa, G., & Ohara, T. (2018). *Comparison of the characteristic of heat transport between non-shear and shear systems at solid-liquid (S-L) interfaces*. *May*, 270–272.

Saleman, A. R. B., Chilukoti, H. K., Kikugawa, G., & Ohara, T. (2019). A molecular dynamics study on the thermal rectification effect at the solid–liquid interfaces between the face-centred cubic (FCC) of gold (Au) with the surfaces of (100), (110) and (111) crystal planes facing the liquid methane (CH4). *Molecular Simulation*, *45*(1). https://doi.org/10.1080/08927022.2018.1535177

Saleman, A. R. b., Chilukoti, H. K., Kikugawa, G., Shibahara, M., & Ohara, T. (2017).

A molecular dynamics study on the thermal energy transfer and momentum transfer at the solid-liquid interfaces between gold and sheared liquid alkanes. *International Journal of Thermal Sciences*, *120*, 273–288. https://doi.org/10.1016/j.ijthermalsci.2017.06.014

Saleman, A. R., Munir, F. A., Rody, M., Zin, M., Yob, M. S., Kikugawa, G., & Ohara, T. (2018). Heat Transport at Solid-Liquid Interfaces between Face-Centered Cubic Lattice and Liquid Alkanes. *Journal of Advanced Research in Fluid Mechanics and Thermal Sciences Journal Homepage*, *44*, 123–130. www.akademiabaru.com/arfmts.html

Saleman, A. R. bin, Chilukoti, H. K., Kikugawa, G., Shibahara, M., & Ohara, T. (2017). A molecular dynamics study on the thermal transport properties and the structure of the solid–liquid interfaces between face centered cubic (FCC) crystal planes of gold in contact with linear alkane liquids. *International Journal of Heat and Mass Transfer*, *105*, 168–179. https://doi.org/10.1016/j.ijheatmasstransfer.2016.09.069

T. Ohara, & D.Suzuki. (2000). Intermolecular energy transfer at a solid-liquid interface. *Microscale Thermophysical Engineering*, *4*, 189–196. https://doi.org/10.1080/10893950050148142

Torii, D., Nakano, T., & Ohara, T. (2008). Contribution of inter- and intramolecular energy transfers to heat conduction in liquids. *Journal of Chemical Physics*, *128*(4), 044504. https://doi.org/10.1063/1.2821963

Torii, D., Ohara, T., & Ishida, K. (2010). Molecular-scale mechanism of thermal resistance at the solid-liquid interfaces: influence of interaction parameters between solid and liquid molecules. *Journal of Heat Transfer*, *132*(January 2010), 012402. https://doi.org/10.1115/1.3211856

Wang, L., Nie, M., & Rumbol, J. (2012). Self-assembled monolayer protective films for hybrid sliding contacts. *Tribology - Materials, Surfaces & Interfaces*, *6*(2), 75–83. https://doi.org/10.1179/1751584X12Y.0000000007